



Shahid Chamran
University of Ahvaz

Journal of Applied and Computational Mechanics



Research Paper

MHD Double-Diffusive Natural Convection in a Closed Space Filled with Liquid Metal: Mesoscopic Analysis

Arun Sathiyamoorthi¹, Satheesh Anbalagan², Hakan F. Öztö^{3,4}, Nidal H Abu-Hamdeh⁵

¹ School of Mechanical Engineering, Vellore Institute of Technology, Vellore, Tamilnadu, 632014, India, Email: arun.smoothi@vit.ac.in

² School of Mechanical Engineering, Vellore Institute of Technology, Vellore, Tamilnadu, 632014, India, Email: satheesh.a@vit.ac.in

³ Department of Mechanical Engineering, Technology Faculty, Firat University, Elazig/Turkey, Email: hfotop1@gmail.com

⁴ Department of Mechanical Engineering, Faculty of Engineering, King Abdulaziz University, Jeddah, 21511, Saudi Arabia

⁵ Department of Mechanical Engineering, Faculty of Engineering, King Abdulaziz University, Jeddah, 21511, Saudi Arabia, Email: nabuhamdeh@kau.edu

Received May 23 2020; Revised August 15 2020; Accepted for publication August 16 2020.

Corresponding author: S. Abbalagan (satheesh.a@vit.ac.in)

© 2021 Published by Shahid Chamran University of Ahvaz

Abstract. In this paper, the lattice Boltzmann approach is carried out to study the double-diffusive natural convection in a space encapsulating liquid metal is presented. The Uniform magnetic field is applied horizontally at the square domain and an insulated rectangular block is kept stationary at the center of the cavity. The linear increment of temperature and concentration is used at the left wall and cold temperature is applied at the right wall. Horizontal walls are adiabatic conditions. Horizontal walls are adiabatic conditions. The numerical analysis is performed at the range of Rayleigh number ($10^3 \leq Ra \leq 10^5$), Lewis number ($2 \leq Le \leq 10$), buoyancy ratio ($-2 \leq N \leq 2$), Hartmann number ($0 \leq Ha \leq 50$) with Prandtl number ($Pr = 0.054$). Results show that the increase in Ra tends to maximize heat and mass transfer rate while increasing Ha , decreases the same. The rise in Le diminishes heat transfer marginally but increasing the mass transfer significantly. The effect of N differs with different operating conditions, in general, the rate of heat and mass transfer is found to decrease with a decrease of N value.

Keywords: Liquid metal, Double-diffusive, Magnetic field, LBM, STR-BGK, Adiabatic block.

1. Introduction

The lattice Boltzmann Method (LBM) has gained a reputation as a potent tool for solving various real-time applications of thermo-fluids. LBM with the Bhatnagar-Gross-Krook (BGK) collision model has gained outstanding acceptance and implications in a fluid flow problem. Many complex and industrial problems were clarified using LBM approaches [1–5]. Liquid metals comprise alloys with low melting points which cause the metal to become a liquid at room temperature. For this unique property, liquid metals are used in many engineering problems, such as metal processing, crystal growth, and in nuclear reactors as a coolant, etc. The low Prandtl number liquids are researched considerably by experiment [6] or numerical simulation [7–10] due to their applications in many fields. These liquids also have high electrical conductivity. Hence the natural convection problem of liquid metal in the presence of a magnetic field is the subject of research [11–14] and mass transfer is also critical in many applications. Therefore the study is also concentrated in mass transfer. Yu et al. [15] investigated natural convective heat-mass flow using liquid Gallium ($Pr = 0.025$) as the working fluid in the cross-section of a cubical closed space with a magnetic effect. They examined over a broad range of relevant non-dimensional parameters. A similar study has been carried out by Hussain [16] using a tilted sinusoidal corrugated porous region filled with a fluid of $Pr = 0.024$. Numerous studies were investigated to examine the flow attributes inside closed domains having realistic industrial needs. [17,18]. For instance, in the design of thermal collectors like solar flat plate heater, advanced building science/physics, aerating and cooling, cooling of electronic gadgets, furnaces, substance handling, drying devices, etc. Prasad et al. [19] analyzed the free convective in a closed space with a central adiabatic block. They carried out the study over the range of Ra , Pr , and block size. Their results proposed a correlation with optimal block size as a function of Pr and Ra . Using the LBM approach Nazir et al. [20] presented the dual-diffusion free convection in an equally closed space with a hot obstacle. The analyses were indicated when $N < 1$, the heat-mass transfer rate decreases with N and for $N > 1$, it augments. Zhang and Che [21] numerically analyzed the free convection in an inclined equal closed space containing nano-fluids with a magnetic effect. The square cavity contains four isothermal square blocks. They have used a multi relaxation time thermal lattice Boltzmann method. Maatki et al. [22] presented the impact of the magnetic effect on three-dimensional flows including heat transfer. Kefayati and Tang [23] used a special fluid called Carreau fluid to investigate the dual-diffusive free convection in a heated domain with an inner low-temperature cylinder and analyzed the effects of various non-dimensional conditions on heat and mass transfer. Muthamilselvan et al. [24] studied the outcome of the non-uniform plate on dual-diffusive free convection with Soret, Dufour effects. They have stated in their results that the vortex viscosity parameter considerably suppresses the heat and mass transfer rate. Mahapatra et al. [25] analyzed the impact of N and body forces on dual-diffusive free



convection in a cavity. This study was further extended by adding a magnetic field and a different cavity angle [26]. Kumar et al. [27] numerically investigated the effect of MHD on Bejan's heat and mass lines in a porous domain by considering Soret and Dufour numbers which show a significant amount of changes in heat-mass transfer and increasing magnetic force reduces the convection rate.

Recently, duct shaped cavity with bottom heating of dual-diffusive mixed convection flow is presented by Hussain et al. [28]. They used Al_2O_3 -water as a working fluid to study the heat and mass transfer characteristics and entropy generation. The finite element method was chosen to solve the governing equations. Further, the same mathematical scheme is used to solve the Fe_3O_4 water nanofluid problem in a cavity with sinusoidal boundaries that were presented [29]. Mehryan et al. [30] investigated the effect of periodic magnetic field in a natural convection flow. The ferrofluid is filled in a square domain. Purushothaman and Satheesh [31] presented a numerical study on two-dimensional steady state natural convection heat transfer in an enclosed domain with sinusoidal wave temperature distribution. The different convection mechanism, such as, Rayleigh number, periodicity, amplitude ratio, phase change and central adiabatic block are varied over the selected range of parameters. Their results show that average Nu number is increased with increase in central block and Ra number. Teamah and Shehata [32] studied the double diffusive MHD natural convection flow in a trapezoidal cavity. The heat and mass transfer were decreased as the increase in inclination angle of the trapezoidal cavity and Hartmann number. They have presented these numerical works into the real-time microorganisms and micropolar based studies. In some other real-time studies, the authors [33-35] presented the natural convective flow and heat transfer of nano-encapsulated Phase Change Materials (PCM) in the cavity. Also, the entropy generation study of mixed convective flow in a vented cavity with inlet and out ports was investigated by considering the inclined magnetic field [36]. At 4% CuO nanoparticle, Nu is found to increase about 25-27% when the absence and presence of a magnetic field. Ratnadeep and Murugesan [37] numerically presented the mixed convective heat-mass transfer study in a backward-facing step channel. Water-ethylene glycol is used as a base fluid and Alumina nanoparticle is mixed at different proportionate. The Taguchi method of L27 orthogonal array is selected to achieve the optimum condition of the selected three levels of six parameters. Out of which, the expansion ratio of the channel is the most influencing parameter followed by the nanoparticle volume fraction. More recently, Yasmin et al. [38] studied with a micropolar fluid flow over a curved stretching sheet. An electrically conducting non-Newtonian fluid is considered hence, the magneto-hydrodynamics effects are incorporated. The magnetic parameter tries to strengthen the concentration than the temperature. It can be noted from the literature that the effect of Ha in the liquid metals study was scarce [15, 16]. Also, the existence of a central insulated block and various boundary conditions are limited investigations in the literature. Hence the explicit motive of this study is to examine the dual-diffusive free-convection flow of liquid metal in equally closed space with a central adiabatic block at the cavity. The impact of Lewis number, Hartmann number, buoyancy ratio, and Rayleigh number on fluid flow are investigated.

2. Mathematical model

"Fig.1" shows the representation of the present numerical work which has the non-dimension of height (H) to width (L) ratio as 1.0. The dimensions of the central insulated block are considered as ' $a \times b = 0.4L \times 0.2L$ '. This means the dimensions of the central block "a" and "b" are 40% and 20% of the length of the computational domain. The right side wall is applied constant temperature (T_c) and low concentration (C_c). The horizontal walls are maintained in adiabatic conditions. The left side wall is applied linearly varying heat ($T_h - (T_h - T_c) y/L$) and mass ($C_h - (C_h - C_c) y/L$) boundary conditions, hence the temperature and concentration have a linear increment along the positive y-axis of the left boundary. The bounce-back boundary conditions are imposed for an internal adiabatic block. Neumann or flux boundary conditions are applied on the four walls of the central rectangular block, therefore, there is no heat transfer from the central adiabatic block to the surrounding fluid medium. The uniform magnetic field (B) passes normal to the left wall of the enclosed domain which is filled with liquid metal ($\text{Pr} = 0.054$) for the present analysis. The two-dimensional (D2), nine-directional (Q9) lattice structure arrangement is considered for this analysis (shown in "Fig. 2"). Single relaxation time (SRT) and (Bhatnagar-Gross-Krook) BGK model [39] is adopted to solve the present problem.

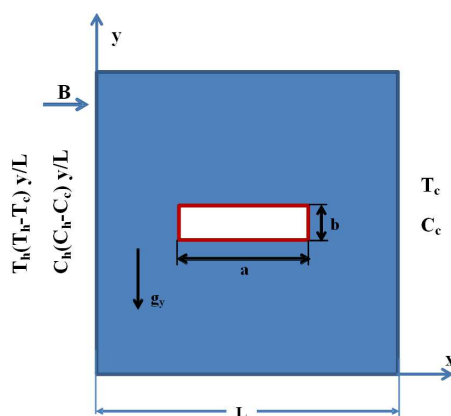


Fig. 1. Physical problem with applied boundary conditions

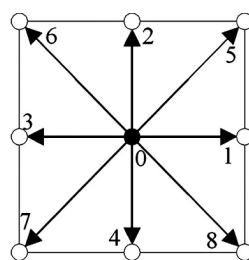


Fig. 2. Lattice structure (D2Q9)



A two-dimensional, incompressible vector ("Eq. 1") and scalar field ("Eq. 2") equations are presented [37],

$$f_i(x + e_i \Delta t, t + \Delta t) = f_i(x, t) - \omega_f [f_i(x, t) - f_i^{eq}(x, t)] + \Delta t F_i. \quad (1)$$

$$g_i(x + e_i \Delta t, t + \Delta t) = g_i(x, t) - \omega_g [g_i(x, t) - g_i^{eq}(x, t)]. \quad (2)$$

where e_i represents the discrete velocity in the respective directions. Lattice time step (Δt) is set to unity. F_i in "Eq. (1)" is a force term which can be written as follows [40]

$$F_i = w_i F \frac{e_i}{e_s^2} \quad (3)$$

where,

$$F = \rho g_y \beta_T \Delta T. \quad (4)$$

Update "Eq. (4)" into "Eq. (3)" the force term is as follows [41]

$$F_i = 3.0 w_i \rho g_y \beta_T \Delta T e_y. \quad (5)$$

In this analysis, the concentration is also considered. Therefore the above equation is impacted by the concentration gradient also.

$$F_i = 3.0 w_i \rho g_y \beta_T \Delta T e_y + 3.0 w_i \rho g_y \beta_c \Delta C e_y. \quad (6)$$

By introducing the Buoyancy ratio (N), "Eq. (6)" is simplified as follows,

$$F_i = 3.0 w_i \rho g_y \beta_T e_y (\Delta T + N \Delta C) \quad (7)$$

Further, the magnetic field is imposed parallel to the x-axis, so the impact of MHD in Eq. (7) and it can be expressed as [42]

$$F_i = 3.0 w_i \rho e_y [(g_y \beta_T (\Delta T + N \Delta C)) - AV]. \quad (8)$$

where,

$$A = Ha^2 \left(\frac{\lambda}{M^2} \right) \quad (9)$$

In "Eq. (9)", Ha represents Hartmann number and it is defined as

$$Ha = BL \sqrt{\frac{\sigma}{\lambda \rho}} \quad (10)$$

f_i^{eq} and g_i^{eq} in "Eq. (1)" and "Eq. (2)" are the equilibrium distribution functions. The equilibrium distribution functions (f_i^{eq} and g_i^{eq}) can be solved using "Eqs. (11) and (12)" [43].

$$f_i^{eq} = w_i \rho \left[1 + 3e_i u + \frac{9}{2} (e_i u)^2 - \frac{3}{2} u^2 \right] \quad (11)$$

$$g_i^{eq} = w_i \rho T [1 + 3e_i u] \quad \text{or} \quad w_i \rho C [1 + 3e_i u] \quad (12)$$

The weight factors (w_i) and lattice velocity (e_i) for D2Q9 model are obtained from the literature [40] and the latest research papers published by the author [5, 43]. The macroscopic properties, such as density (ρ), velocities (u and v), temperature (T), and concentration (C) are calculated using the following equations ("Eqs. 13-15").

$$\text{Flow density: } \rho = \sum_i f_i \quad (13)$$

$$\text{Momentum: } \rho u(x, t) = \sum_i f_i e_i \quad (14)$$

$$\text{Species: } T = \sum_i g_i \quad \text{or} \quad C = \sum_i g_i \quad (15)$$

2.1 Stream Function

The streamline contours (ψ) are plotted from respective velocities (U, V). The following equation is used to calculate the stream function [42].

$$\frac{\partial^2 \psi}{\partial X^2} + \frac{\partial^2 \psi}{\partial Y^2} = \frac{\partial U}{\partial Y} - \frac{\partial V}{\partial X} \quad (16)$$



In the present work, the clockwise circulation of streamline contours is considered a negative sign of ψ and vice versa. The average Nu and Sh are determined to understand the physical behaviors of total heat and mass transfer, respectively. It is obtained by integrating the local Nu and/or Sh at hot walls by the following expressions

$$Nu = \left(-\frac{\partial T}{\partial X} \right)_{X=0} ; \quad Sh = \left(-\frac{\partial C}{\partial X} \right)_{X=0} \quad (17)$$

$$avg. Nu = \int_0^1 Nu dy ; \quad avg. Sh = \int_0^1 Sh dy \quad (18)$$

2.2 Boundary Conditions

Based on D2Q9 lattice structure arrangement the unknown distribution functions at the particular directions are specified by given in Ref. [43]. The bounce-back boundary condition is applied including a central rectangular block.

For linearly heating left wall the following conditions are used.

$$g_1 = (T_h - (T_h - T_c)y/L) \times (w_1 + w_3) - g_3,$$

$$g_5 = (T_h - (T_h - T_c)y/L) \times (w_5 + w_7) - g_7,$$

$$g_8 = (T_h - (T_h - T_c)y/L) \times (w_8 + w_6) - g_6,$$

For the concentration field also the above boundary conditions are applied.

3. Methodology

The double-diffusive free convection flow is investigated with the effect of the magnetic field using LBM. This study is performed for the selected range of non-dimensional parameters to investigate the heat-mass transfer in the closed space working with a liquid metal of $Pr = 0.054$. The convergence criteria of this numerical study are fixed as $|\varphi_{n+1} - \varphi_n| \leq 10^{-6}$. The numerical code is developed using "C" programming language. Detailed procedures followed in the present work are reported by the author in their recent publication [43].

4. Results and Discussion

4.1 Grid Independent Test and Validation

To ensure that the present numerical results are independent of grid size, the computations are performed for different grid sizes. Fig. 3a shows avg. Nu and Sh for different grid sizes for different operating conditions. Also, Table 1 presents the same for the selected grid sizes. From these analyses, beyond the grid size of 181×181 , the obtained results are found insignificant variation with the higher grid sizes. Thus, the grid size of 181×181 is taken to perform a further numerical study. Fig. 3b shows the structured grid of 181×181 of uniform spacing between the nodes. To validate the present code, the streamline and isothermal contours obtained for $Ha = 50$, $Pr = 0.025$, $Ra = 10^5$ when the left wall is linearly heated, and right wall is at cold temperature, are compared with reported literature [13] and, the results are presented in Fig. 4a. Also to ensure flawless of the developed code another comparison [20] is carried out and it is shown in Fig. 4b. From these comparisons, it sounds the present study agrees well with the reported literature.

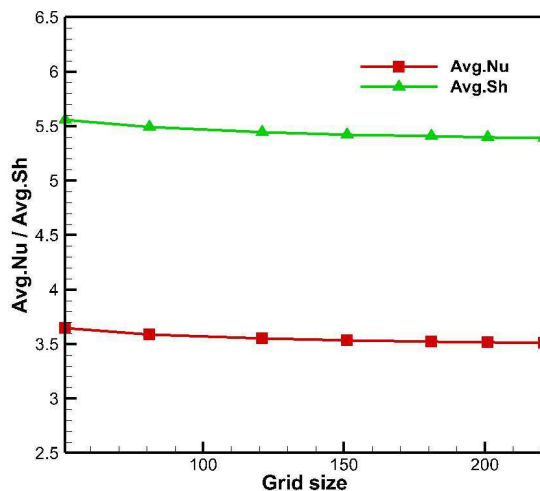


Fig. 3a. Average Nusselt number and Sherwood number for $Ra = 10^5$, $Le=2.0$, $N = 1.0$, $Ha = 30$.

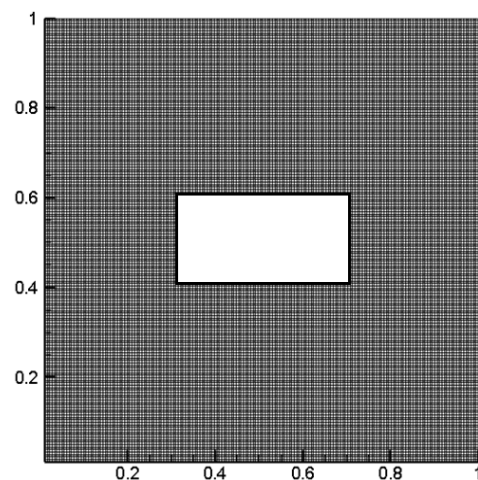


Fig. 3b. A view of the utilized grid with a size of 181×181



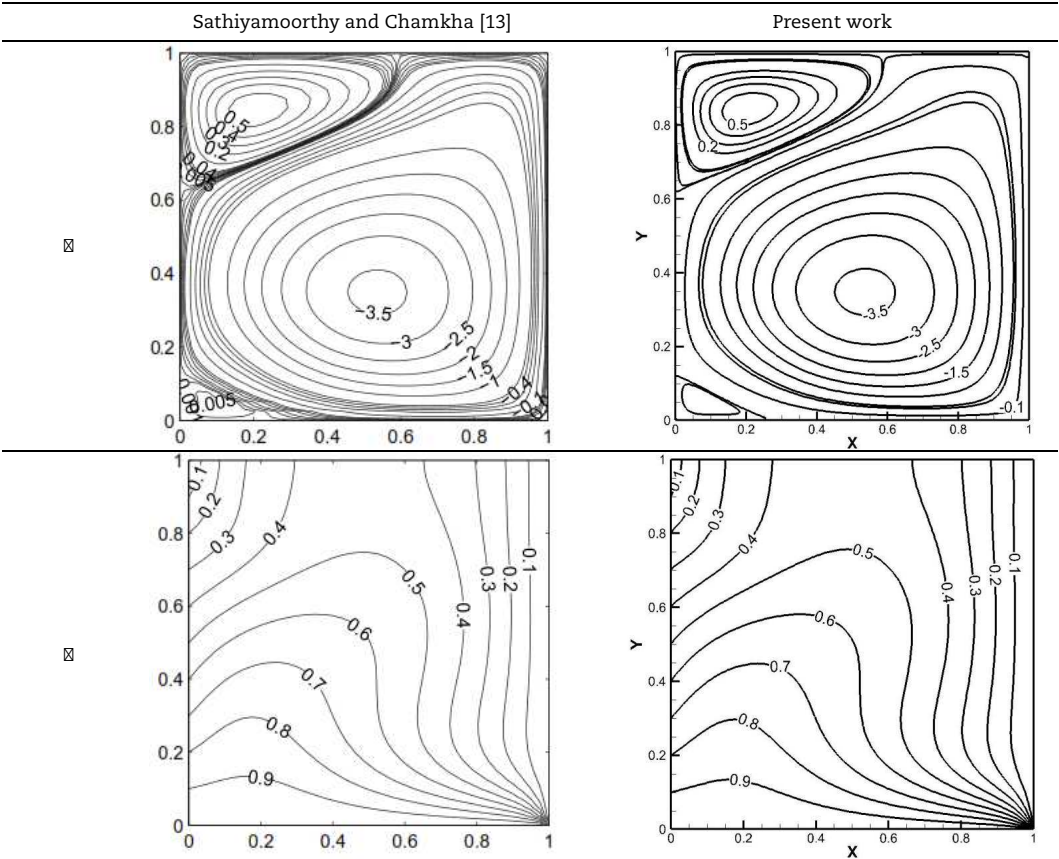


Fig. 4a. Streamline and isotherms comparison with Sathiyamoorthy and Chamkha [13].

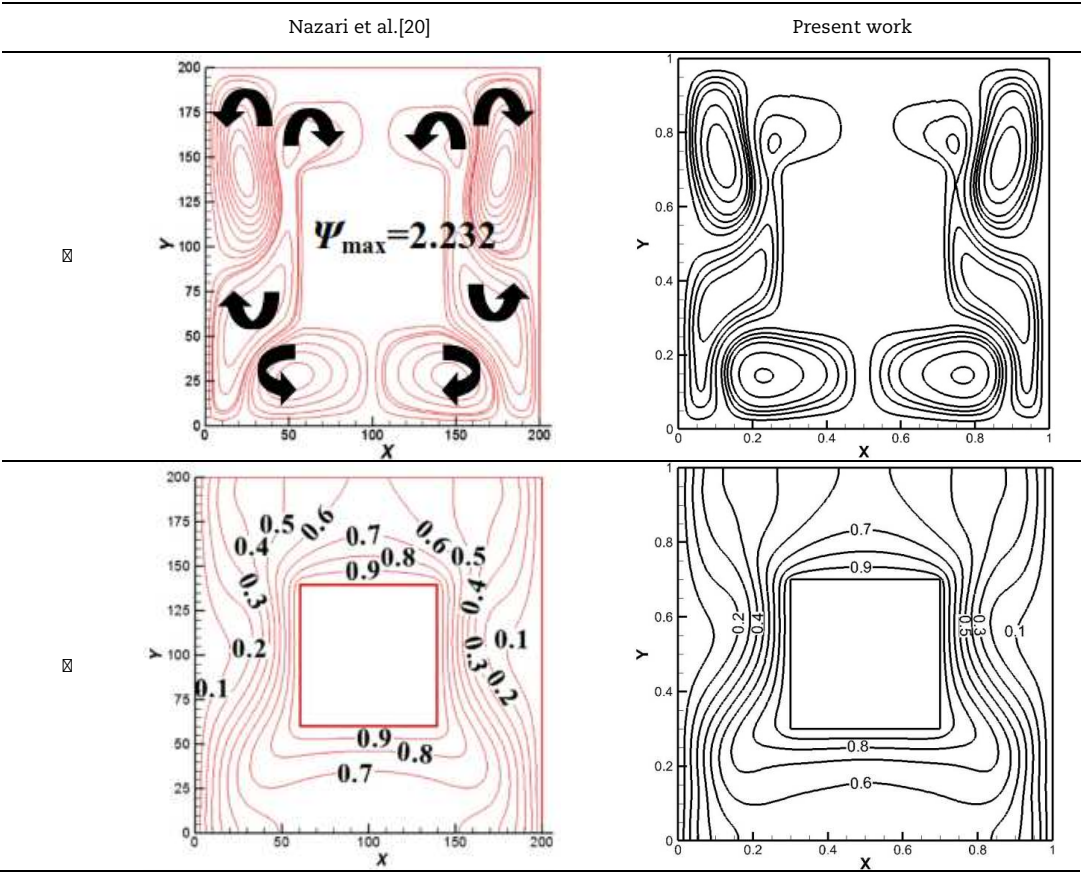
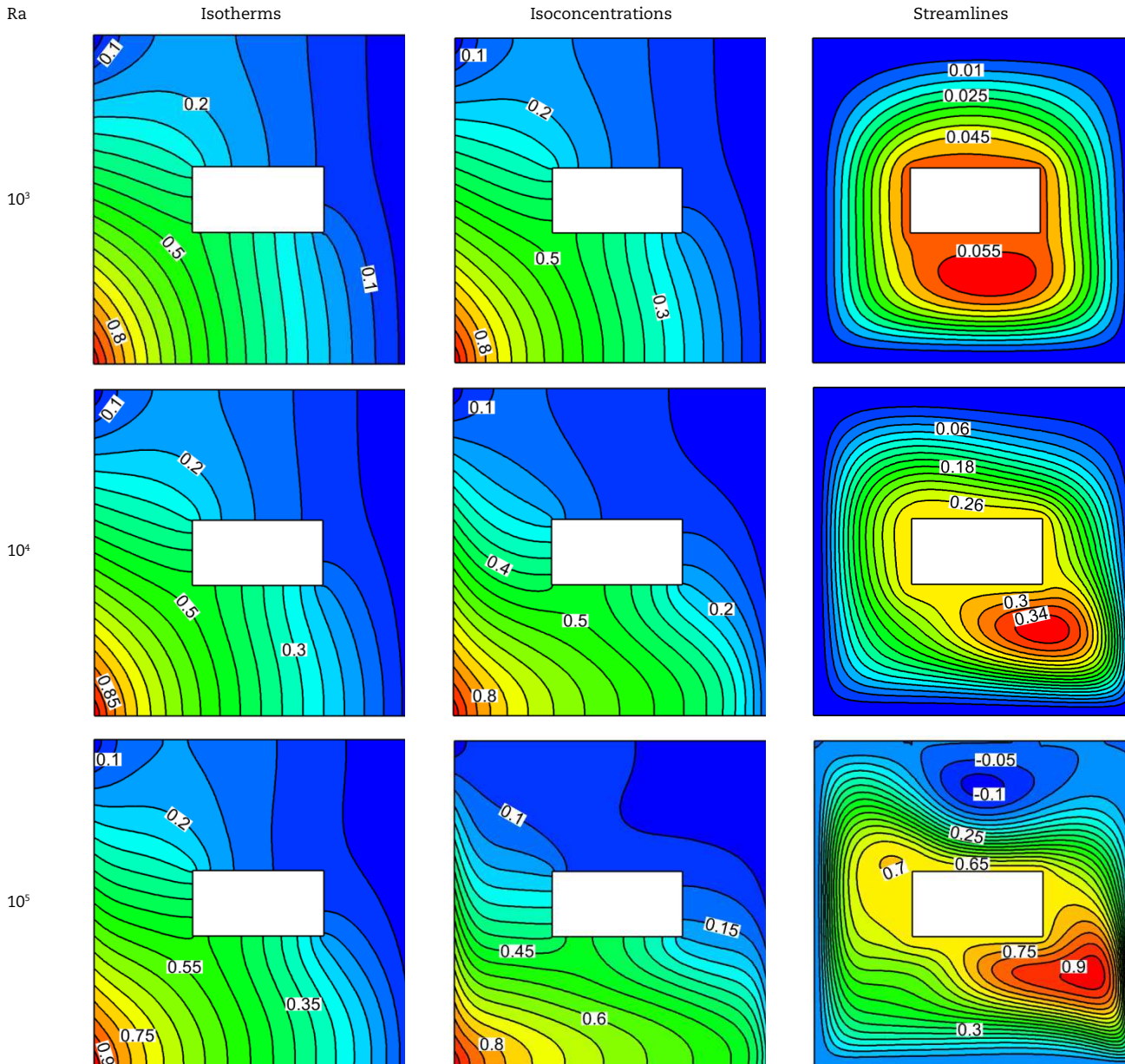


Fig. 4b. Streamline and isotherms comparison with Nazari et al [20].



Table 1. Grid independence study.

Grid size	Ra = 10^4		Ra = 10^5	
	Avg. Nu	Avg. Sh	Avg. Nu	Avg. Sh
101 x 101	1.168	3.176	2.471	8.529
121 x 121	1.163	3.158	2.455	8.496
151 x 151	1.158	3.140	2.439	8.457
181 x 181	1.155	3.127	2.425	8.424
201 x 201	1.154	3.125	2.423	8.423

**Fig. 5.** Isotherms, isoconcentrations, streamlines for different Ra when $N = -2$, $Le = 6$ and $Ha = 30$.

Double-diffusive free convection in an equally spaced enclosure with the presence of a central insulated rectangular block is examined, numerically for selected parameters.

"Fig. 5" shows the isotherms, isoconcentrations, and streamline contours obtained for various Ra at $N = -2.0$, $Le = 6$ and $Ha = 30$. For $Ra = 10^3$, the isotherms and isoconcentrations diffuse from the bottom left wall to the right wall of the cavity. The streamline contours form the noncircular pattern due to the presence of the adiabatic block in the middle of the enclosure. Due to different boundary conditions and block, the secondary complete circulation forms at the bottom end of the block. The $\psi_{\max} = 0.055$ is observed in this second cycle. The positive value of ψ indicates the rotation of the fluid is in a counter-clockwise direction. The opposing buoyancy force may influence the course of the fluid. When Ra is increased to 10^4 , the isotherms show insignificant variation with $Ra = 10^3$. The diffusion rises slightly which can be observed around the bottom left side of the block. For example, the constant diffusion line of 0.45 is increased. In concentration, the increase in convection can be observed. Most of the contour lines are slanting from normal to the horizontal wall of the cavity to parallel to the horizontal walls. This transition is due to the dominant convection regime in the fluid flow inside the cavity. The strength of circulation increases in the streamline contours, which can be noted by observing the streamlines, is getting densely packed. The ψ_{\max} value increases significantly to 0.34. The



secondary vortex due to an increase in fluid flow circulation tends to move towards the right side of the cavity. Further increasing $Ra = 10^5$, the changes observed in isotherms is more extensive when compared with previous Ra . And the isoconcentrations and streamline patterns show more substantial differences in the earlier cases. In isoconcentrations, the boundary layer thickness around the walls of the cavity gets much denser, and the constant lines are slanted so much as parallel to the horizontal walls of the cavity. This shows the high convection rate in the cavity. In the streamline, the increase in Ra further produces very dense streamlines that incur the more considerable increase in the strength of the circulation. There is the formation of another secondary vortex around the top left of the block. The first secondary vortex moves towards the right side of the cavity, and its patterns also change from the oval shape. The ψ_{\max} is 0.9, which is almost 200% increase when compared with ψ_{\max} obtained when $Ra = 10^4$. There is also the formation of the ternary vortex near the top wall of the cavity which flows in the clockwise direction.

"Fig. 6" shows the horizontal and vertical midplane velocity profile. The increase in Ra causes the velocity profile to increase considerably. At $Ra = 10^3$, the horizontal velocity profile shows that at the top of the cavity the increment is higher, however, at the bottom of the cavity, the velocity due to $Ra = 10^4$ is maximum. The same phenomenon is not observed in the vertical velocity profile. "Table 2" displays the avg. Nu and avg. Sh values obtained for different Ra values. By following the "Table 2", it can be found that the increase in Ra value augments both heat and mass transfer significantly. Because of higher N and Le value, the mass transfer rate increases higher than the heat transfer rate. The increased percentage of heat transfer rate is around 30% for $Ra = 10^3$ and 10^5 , whereas the percentage increase in the mass transfer rate is about 80% for the same conditions of Ra .

"Fig. 7" illustrates the isotherm, isoconcentrations, and streamlines obtained for different Ra and Ha at $N = 2$, $Le = 4$. Since the buoyancy ratio is positive, both the thermal and solutal gradient aids in the fluid flow for all the conditions. The Lewis number is chosen to be more than unity, which increases the solutal diffusion rate when compared with the thermal diffusion rate in the system. For $Ha = 0$ and $Ra = 10^3$, the temperature and concentration diffuse from the higher region to lower region, due to the linear boundary condition the isotherms and isoconcentrations contours show the profile from the bottom of the left wall to the right wall. Due to linearly varying boundary conditions at the left wall and the constant boundary condition at the right wall, the fluid rises along the side of the left wall and flows down along the cooled right wall and forms clockwise rotation in the cavity.

The presence of the adiabatic block at the center of the cavity makes the circulation of the fluid flow not to be a precisely circular shape. It can be noted that the diffusion rate decreases when Ha increases. Due to low Ra , the isotherms show only slight variations even when Ha is increased to 50. And in isoconcentrations, the constant line 0.3 which almost covers 60% of the cavity when $Ha = 0$, but when Ha has increased this area starts to diminish. This shows the reduction of the diffusion rate. In streamline patterns, the ψ_{\max} value is significantly reduced by the increase of Ha . The formation of the secondary flow pattern also observed at the bottom side of the adiabatic block. When Ra is increased to 10^4 , the thermal gradient increases and causes the convection rate to improve significantly.

The thermal and solutal boundary can be seen very dense near the left wall for half of the cavity height because of the linear boundary. In isotherms, the constant line 0.3 diffuses almost to the half of the cavity when $Ha = 0$, and this diffusion decreases with increasing Ha . When Ha is 0, the iso-concentration lines near the left wall are increasing sharply due to the higher convection rate. And for higher Ha values, it can be observed there are no such sharp increases. The boundary layer thickness also decreases significantly. This shows the effect of the increasing magnetic field massively impacts the heat and mass diffusion rate. The ψ_{\max} is 3 for $Ha = 0$, for the same Ha when Ra is 10^3 the ψ_{\max} is 0.75. When Ha is increased, it is observed that the strength of the circulation of the fluid reduces significantly. The magnetic field when increased dramatically affects the strength of the distribution of the liquid. And the flow pattern near the block also changes with rising in Ha . This same phenomenon also observed in lower Ra , but for $Ra = 10^4$ secondary cell structure is slightly inclined towards the left wall side. When Ra is further increased to 105, it can be observed from the contours the diffusion is maximum when Ha is 0 and reduces when Ha increases. The same is found for other Ra values also, but because of higher Ra , the convection rate is remarkably higher when compared to different Ra values. As observed in previous cases the ψ_{\max} value keeps on decreasing with increasing Ha for this case also. And there is a formation of a secondary vortex that circulates in a counterclockwise direction near the top left corner where the thermal and concentration are minimum. The ψ_{\max} value of this secondary vortex increases with an increase in Ha value. It shows that for aiding flow condition the ψ_{\max} value of the secondary vortex which flows in the opposite direction to the primary vortex increases with an increase in Ha . "Fig. 8" represents the horizontal and vertical midplane velocity profile for different Ha and $Ra = 10^5$ at $N = 2$ and $Le = 4$. From the profiles, it is noted that the velocity of the fluid both in horizontal, vertical direction reduces with Ha in the enclosure.

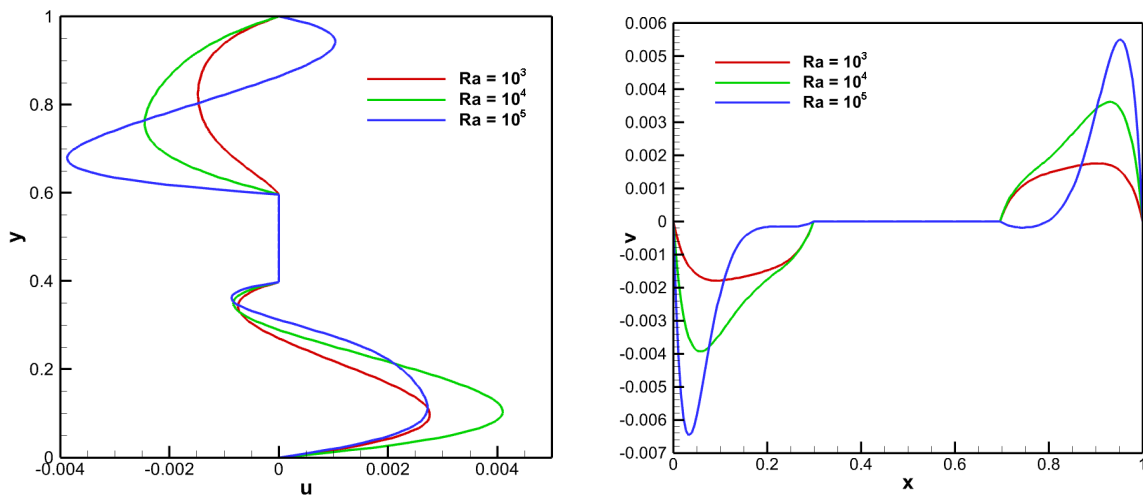
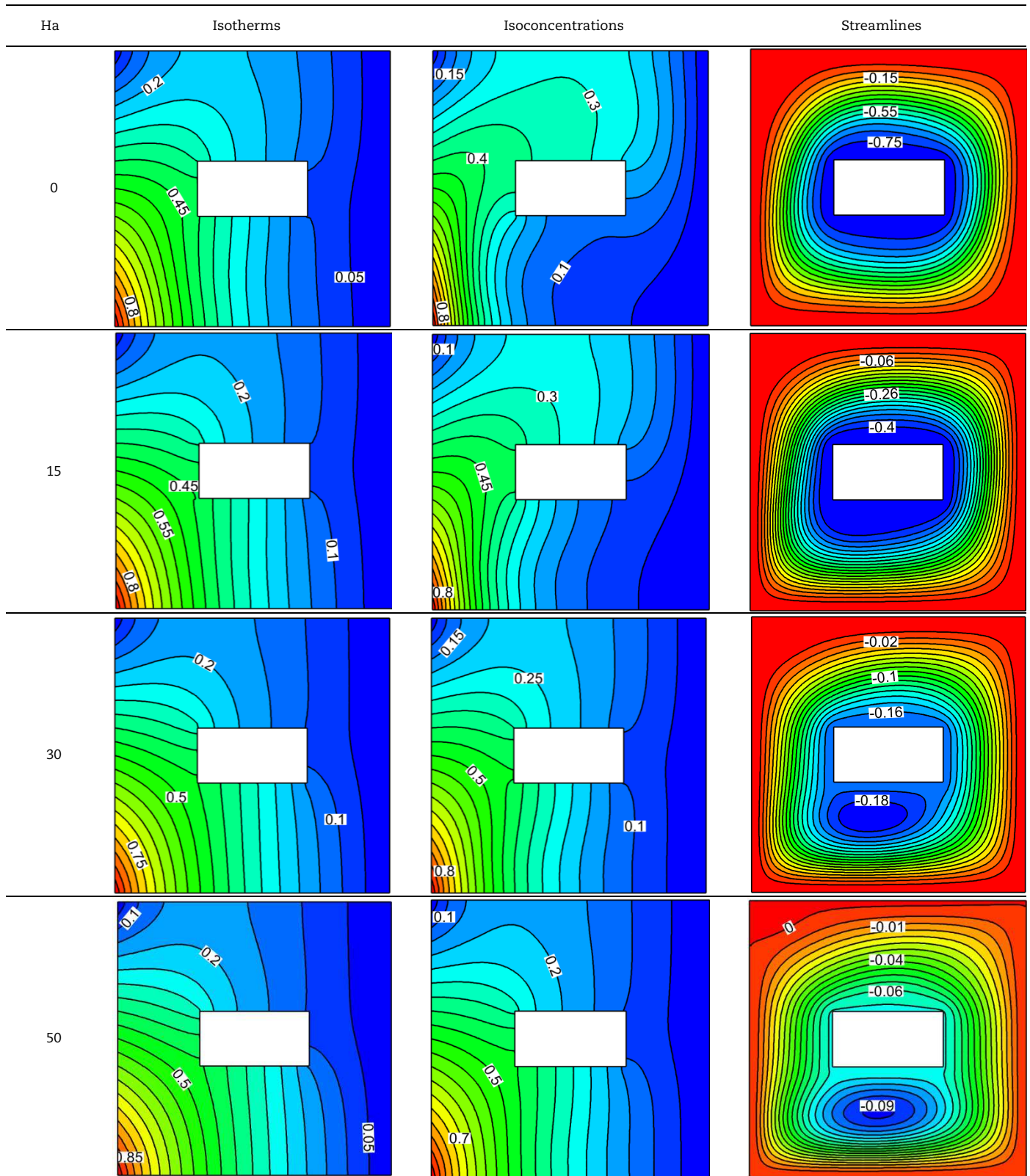


Fig. 6. Horizontal mid plane velocity and vertical mid plane velocity for different Ra when $Le = 6$, $N = -2$ and $Ha = 30$.



Table 2. Avg. Nu and avg. Sh for different Rayleigh number when $Le = 6$, $N = -2$ and $Ha = 30$.

Ra	Avg. Nu	Avg. Sh
10^3	0.437037	0.479636
10^4	0.477207	0.992367
10^5	0.618344	2.341534

a) $Ra = 10^3$ **Fig. 7.** Isotherms, isoconcentrations, streamlines for different Ha when $N = 2$, $Le = 4$ and different Rayleigh numbers a) $Ra = 10^3$, b) $Ra = 10^4$, c) $Ra = 10^5$ 

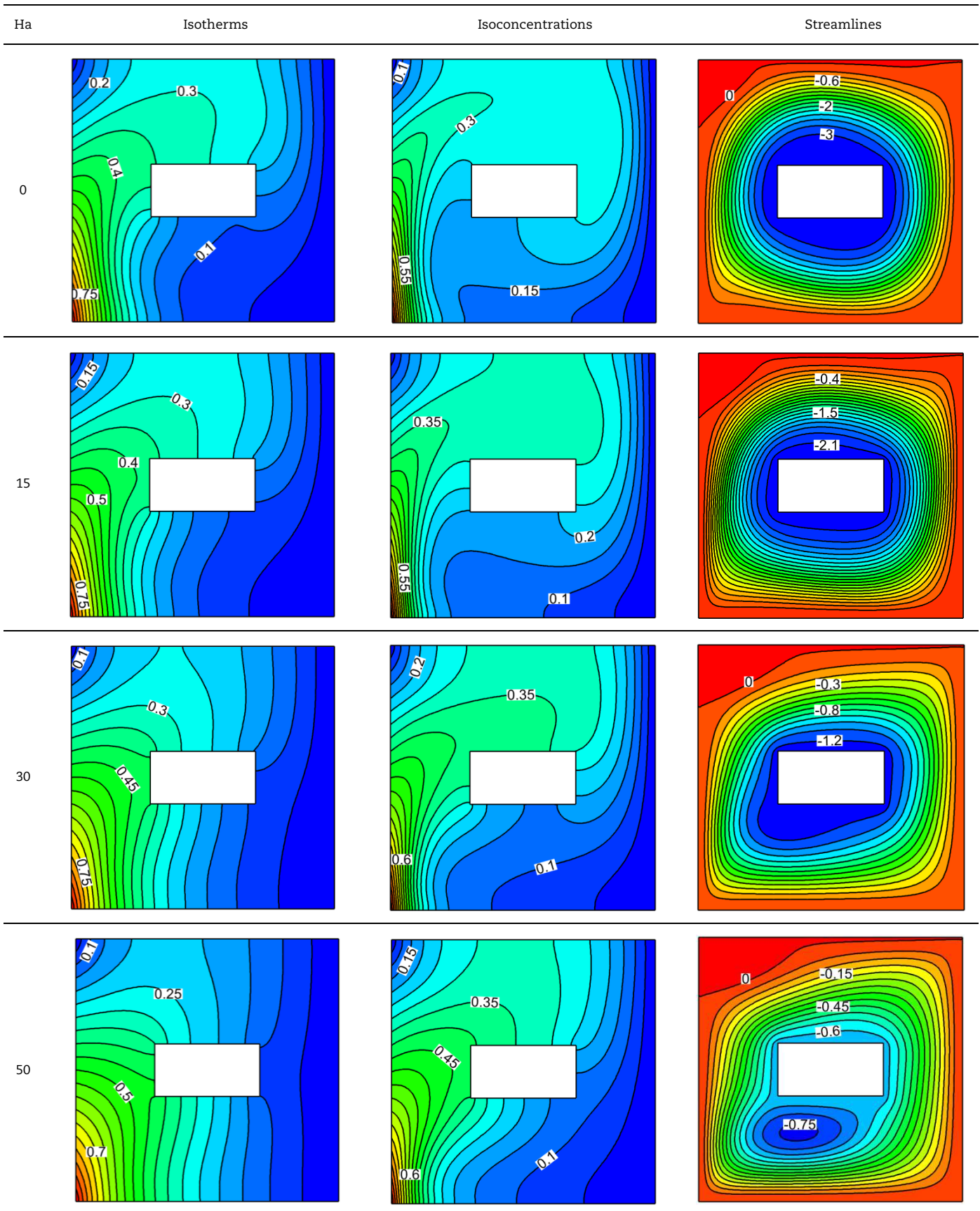
b) $Ra = 10^4$


Fig. 7. Isotherms, isoconcentrations, streamlines for different Ha when $N = 2$, $Le = 4$ and different Rayleigh numbers a) $Ra = 10^3$, b) $Ra = 10^4$, c) $Ra = 10^5$



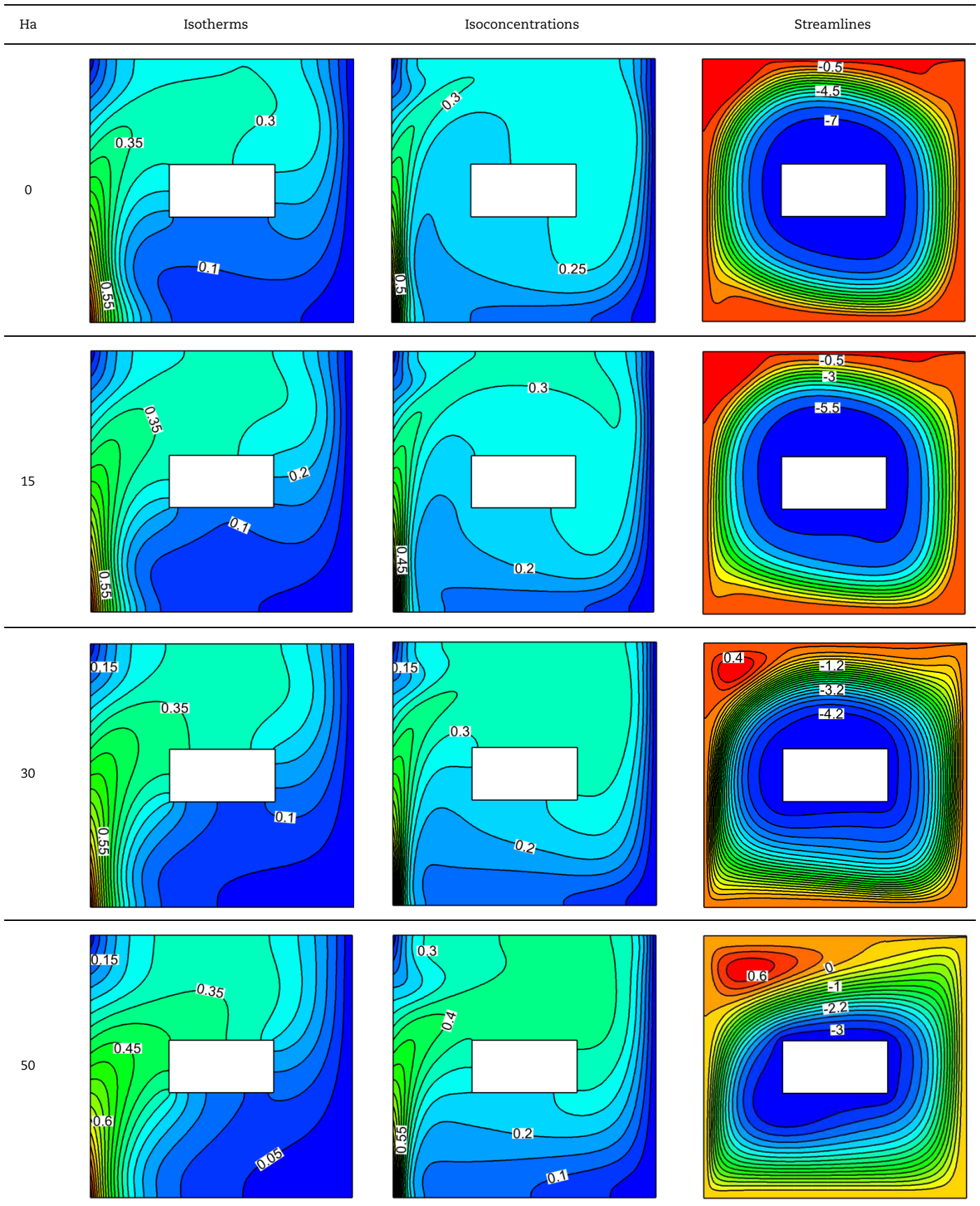
c) $Ra = 10^5$ 

Fig. 7. Isotherms, isoconcentrations, streamlines for different Ha when $N = 2$, $Le = 4$ and different Rayleigh numbers a) $Ra = 10^3$, b) $Ra = 10^4$, c) $Ra = 10^5$



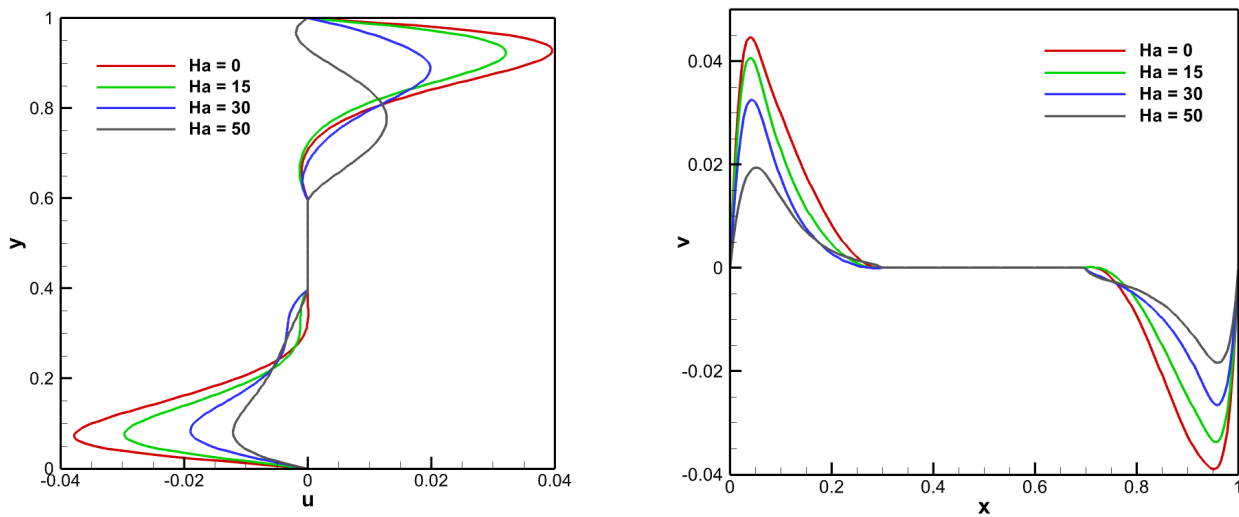


Fig. 8. Horizontal midplane velocity and vertical midplane velocity for different Ha when $Le = 4$, $N = 2$ and $Ra = 10^5$

“Fig. 9” compares the isotherms, iso-concentration, and streamlines for different Lewis numbers when $Ra = 105$, $N = 2$, and $Ha = 15$. It can be noted from the results that the increase in Lewis number impacts the heat diffusion and fluid flow pattern slightly. The heat diffusion around the cavity slowly decreases with Le . And in streamline pattern, the opposing secondary circle with the strength of 0.5 observed on the top left corner was found for $Le = 2$ which is not visible on higher Le . The ψ_{\max} values also degenerate slightly for higher Le values. The isoconcentrations, however, shows massive change with the increment of Le . The boundary layer thickness gets denser around the walls and also the diffusion pattern increases very sharply. The constant 0.3 contour diffuses around the middle of the block when $Le = 2$ and when Le is raised, the same line shows it covered more length. The same can be observed for other constant lines also which shows the augmentation of the mass diffusion rate.

“Fig. 10” shows the horizontal midplane velocity along the y -axis and vertical midplane velocity along the x -axis. It can be observed that at the bottom of the cavity u velocity for Le values is decreasing much when compared to $Le = 2$. But at the top of the cavity, there was a slight change at $Le = 4$, u velocity does not decrease as much as observed on the lower side of the cavity. The same phenomenon can be seen in v velocity also. Whereas at the cold side of the cavity, the v velocity of other Le values reduces much when compared to $Le = 4$, and at the right side the decrease is gradual. This kind of situation might be happening due to the different boundary conditions applied to the opposing cavity walls. However, it can be understood that increasing in Le value affects the velocity of the fluid to reduce. Even though the reduction is minimal, it can be observed in Fig 10. “Table 3” shows the avg. Nusselt and Sherwood numbers obtained for different Ra and Le when $Ha = 15$ and $N = 2$ and -2 . From the tabular column results it is noted that for $Ra = 10^3$, the average Nusselt number increases marginally when Le is increased. This marginal increase is observed for $N = 2$ conditions only. For other conditions, the heat transfer rate decreases with an increase in Le value. And for higher Ra values this decreasing effect also observed to diminish. For $N = 2$ and $Ra = 10^4$, the decrement of 26.34% is observed between $Le = 2$ and 10. For a similar condition for higher $Ra = 10^5$, the percentage decrease is 18.93%. But for the opposing buoyancy force ($N = -2$), for the same conditions, the decrease percentage obtained is 23.08% and 49.09% respectively. From this, it can be understood that for $N = -2$, for higher Ra values the heat transfer rate decreases greater for different Le value when compared with lower Ra values. As already mentioned in the previous explanation that mass diffusion increases with increment in Le values can also be attested by observing the avg. Sh values displayed in the tabular column. When the Le increases, irrespective of any conditions the mass diffusion rate increases. And also for all the conditions, the mass transfer is higher when compared with heat transfer.

Table 3. Avg. Nu and Sh for different Ra and Le when $Ha = 15$ and $N = 2.0$ and -2.0 .

$Ha = 15$	$N = 2$			$N = -2$		
	$Ra = 10^3$	$Ra = 10^4$	$Ra = 10^5$	$Ra = 10^3$	$Ra = 10^4$	$Ra = 10^5$
Avg. Nu	$Le = 2$	0.3780	0.6777	1.5858	0.4532	0.6253
	$Le = 4$	0.3788	0.5880	1.4046	0.4511	0.5425
	$Le = 6$	0.3800	0.5486	1.3301	0.4491	0.5100
	$Le = 8$	0.3813	0.5162	1.3034	0.4473	0.4923
	$Le = 10$	0.3825	0.4992	1.2856	0.4458	0.4810
Avg. Sh	$Le = 2$	0.3843	1.1381	2.3093	0.4767	0.9182
	$Le = 4$	0.5007	1.5703	3.0317	0.5333	1.1415
	$Le = 6$	0.6456	1.8533	3.5335	0.5910	1.2984
	$Le = 8$	0.7777	2.0721	3.9696	0.6447	1.4218
	$Le = 10$	0.8925	2.2551	4.3508	0.6936	1.5249



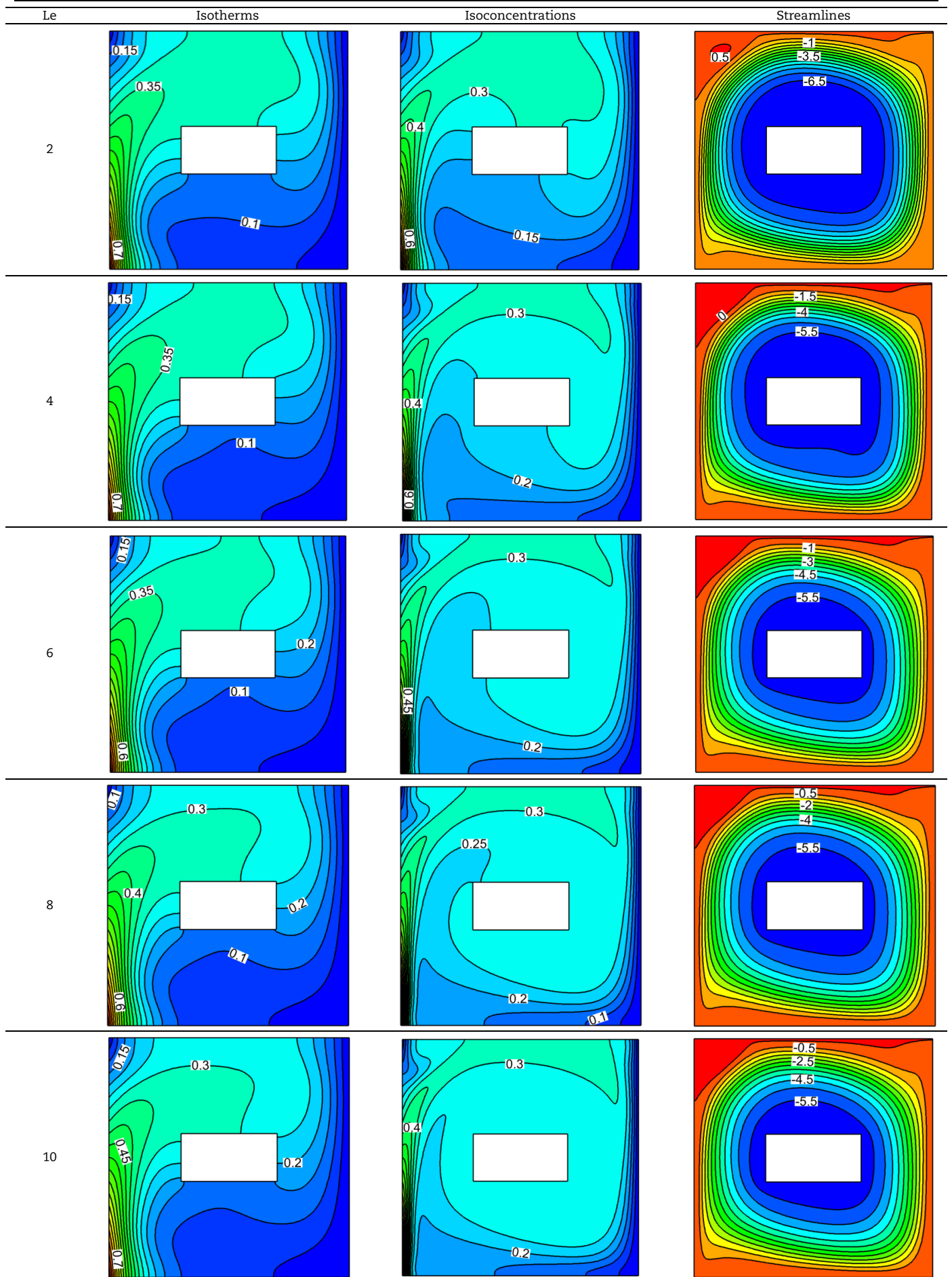


Fig. 9. Isotherms, isoconcentrations, streamlines for different Lewis numbers when $N = 2$, $Ha = 15$ and $Ra = 10^5$



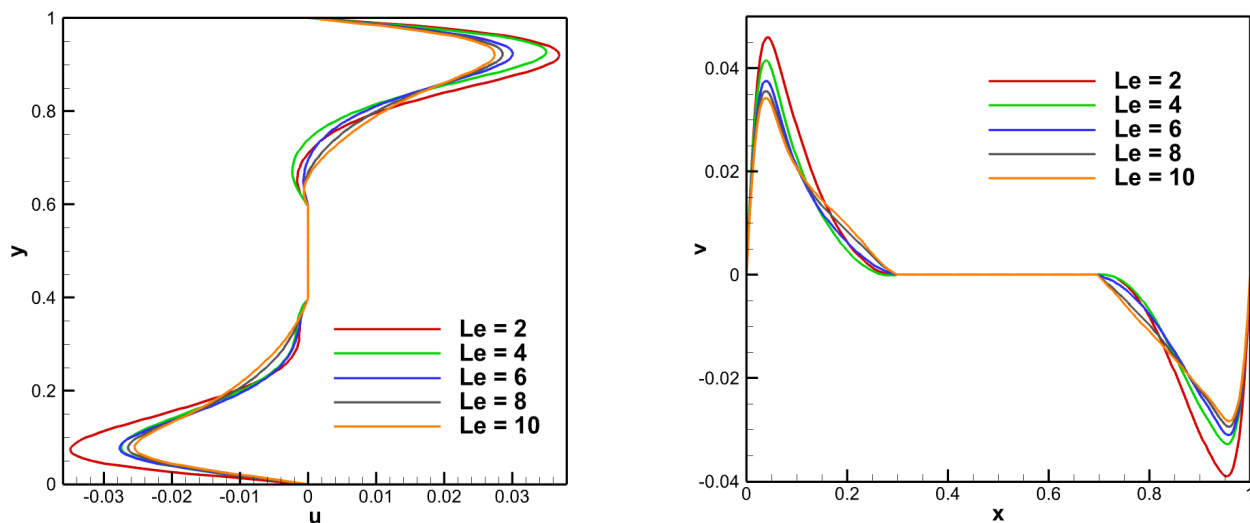


Fig. 10. Horizontal mid plane velocity and vertical mid plane velocity for different Le when $Ha = 15$, $N = 2$ and $Ra = 10^5$.

"Fig. 11" shows the isotherm, isoconcentrations, and streamlines obtained for different Buoyancy ratio when $Le = 2$, $Ha = 0$ and $Ra = 10^5$. The positive N value augments the effects of solutal and thermal gradients which strengthen the fluid flow circulation. And in the negative N value, the thermal and solutal gradients oppose each other which interns affect the fluid flow circulation inside the cavity. When N value is decreasing, from the diffusion of the gradients in the contours both in isotherms and isoconcentrations that the convection rate is getting lower. And by observing the reduction in the ψ_{max} value in the streamline contours also concurs with the previously mentioned point. And the results obtained for opposing buoyancy force is substantially different from the aiding flows. When N is positive, the heat and mass diffuse from the lower left side of the cavity towards the top wall and diffusion occurs from the right wall towards the bottom wall of the cavity which in turns the produce the clockwise direction of the fluid inside the enclosure. And when N is negative, the process occurs in the reverse direction which causes the flow to be reversed. So the isotherms and iso-concentration contours obtained for negative N value appear entirely different from the positive case. The streamline pattern also changed considerably. In the positive case, the fluid flow is in a circle and not much disturbed by the presence of the adiabatic block. There is also the formation of the secondary circle on the left side of the cavity. It is also observed that by further increasing the N value in the negative direction the solutal gradient dominates thoroughly and which leads to the augmentation effects. The ψ_{max} value also increases from 1.4 to 2.0 by increasing N value from -1.5 to -2, which happens due to the decrease in the opposing effects caused by thermal and solutal gradients. Fig.12 displays the horizontal and vertical midplane velocity profile. The horizontal and vertical velocity of the fluid decreases with a decrease in buoyancy ratio. When N value is positive, the direction of the velocities is negative which represents the clockwise rotation of the fluid and when N is negative, as mentioned in the streamline patterns the velocity direction reverses. The increase of negative N value causes the velocity of the fluid to increase in a positive direction. Even though the increment is in the meager amount, it is observed in both horizontal and vertical velocity profiles.

"Table 4" shows the average Nusselt and Sherwood number for different Ra and N when $Ha = 0$ and $Le = 2$. When $Ra = 10^3$, the avg. Nu decreases with decreasing N value but starts to increase later. The same was observed in avg. Sh also but for various N values. In general, it can be understood from the multiple results that $Ra = 10^3$, the convection regime is not stronger. So when Ra increased further the heat and mass transfer rate increases. Similarly, the effects of the Buoyancy ratio also differ on various Ra values. For $Ra = 10^4$ and 10^5 , the convection rate of heat and mass transfer gradually decreases with decreasing N value. However, when $N = -2$, the heat and mass transfer rate starts to increase again, this process was observed very early for $Ra = 10^3$.

"Fig. 13" shows the effect of aiding ($N = 2.0$) and opposing ($N = -2.0$) Buoyancy ratio on the average Nusselt number and Sherwood number for all the operating conditions taken for study ($10^3 \leq Ra \leq 10^5$), ($2 \leq Le \leq 10$), and ($0 \leq Ha \leq 50$). When $Ra = 10^3$, for all the conditions the heat transfer rate does not change much with increasing Le and Ha . And heat transfer rate due to the opposing force is slightly higher. This is not the case in the solutal diffusion rate. The avg. Sh values increase with an increase in the Lewis number. The mass diffusion rate obtained for positive N value is found to be higher when compared to negative N value. The expansion of the magnetic field dramatically influences the diffusion rate. For higher Ha values the interference of the magnetic field causes the mass diffusion rate to not increase significantly as Le increases which are observed when $Ha = 0$. And also the avg. Sh of opposing Buoyancy tends to be slightly higher than the positive. When Ra has further increased the heat diffusion rate decreases with an increase in Le and Mass transfer rate increases with an increase in Le number.

Table 4. Avg. Nu and Sh for different Ra and N when $Ha = 0$ and $Le = 2.0$.

N	$Ra = 10^3$		$Ra = 10^4$		$Ra = 10^5$	
	Avg. Nu	Avg. Sh	Avg. Nu	Avg. Sh	Avg. Nu	Avg. Sh
2.0	0.382095	0.505214	0.866838	1.300450	1.693659	2.315334
1.5	0.376804	0.463704	0.822001	1.246626	1.625723	2.204975
0.2	0.382377	0.377924	0.657976	1.044323	1.406718	1.871057
-1.5	0.455093	0.481517	0.591820	0.837791	0.886493	1.537624
-2.0	0.483202	0.549944	0.720793	1.121059	1.185364	2.122539



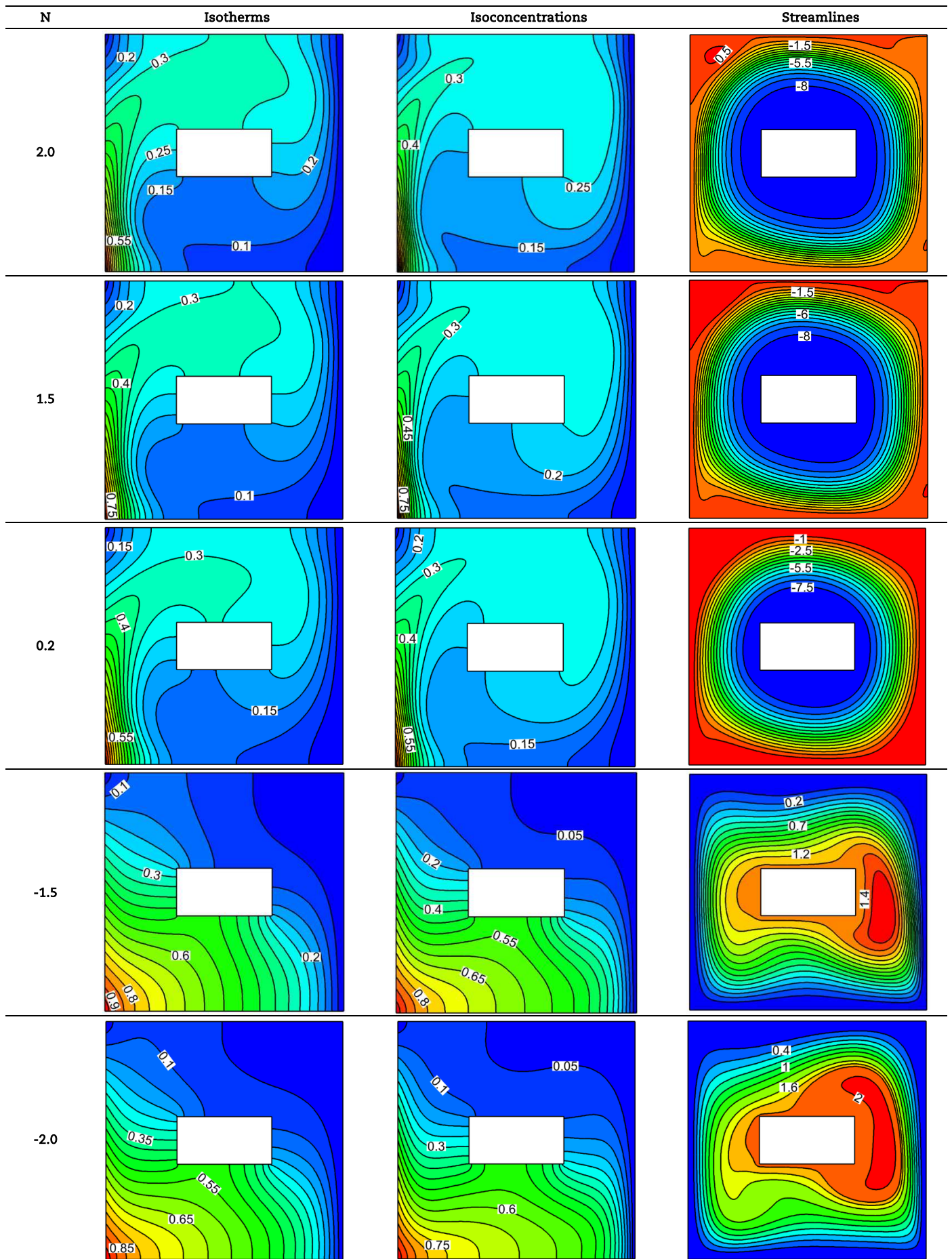


Fig. 11. Isotherms, isoconcentrations, streamlines for different Buoyancy ratio, $Le = 2$, $Ha = 0$ and $Ra = 10^5$



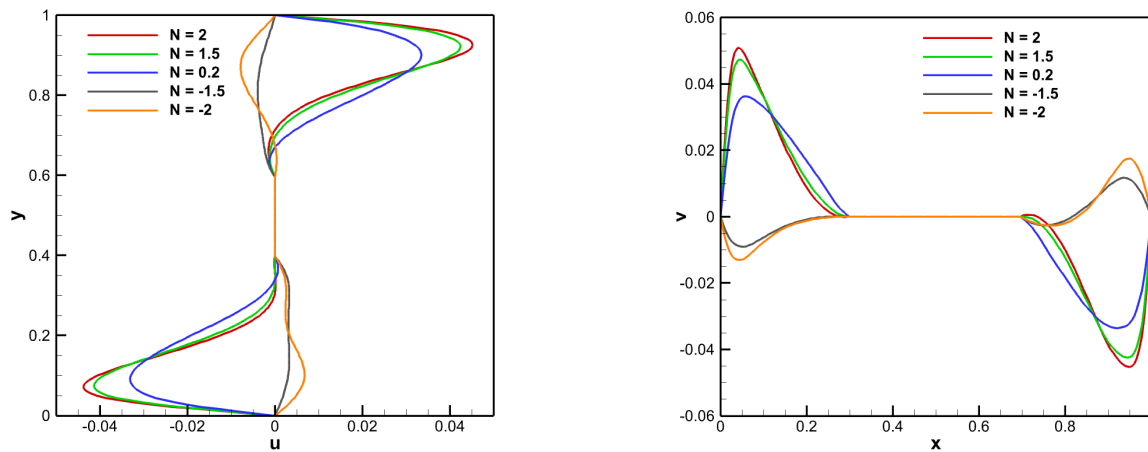


Fig. 12. Horizontal midplane velocity and vertical midplane velocity for different Buoyancy ratio when $Ha = 0$, $Le = 2.0$ and $Ra = 10^5$.

5. Conclusions

The double-diffusive MHD natural convection in a closed space filled with liquid metal is studied using Lattice Boltzmann Method. Effects of Rayleigh number ($10^3 \leq Ra \leq 10^5$), Lewis number ($2 \leq Le \leq 10$), buoyancy ratio ($-2.0 \leq N \leq 2.0$), Hartmann number ($0 \leq Ha \leq 50$), and Prandtl number ($Pr = 0.054$) on the heat and mass transfer is presented. Results are compared with the reported literature and agree well with them. From the present numerical results, some of the important conclusions are summarized below.

- The increase in Ra tends to amplify the heat and mass transfer rate.
- For higher Ra number, the fluid circulation increases. When Ra has increased to 10^5 the ψ_{\max} value increase 200% when compared with ψ_{\max} obtained for $Ra = 10^4$.
- The increase in Hartmann number causes the heat and mass diffusion rate to decrease for all Rayleigh numbers.
- The strength of circulation decreases with an increase in the Hartmann number. However, it is observed that for aiding flow condition the ψ_{\max} value of the secondary vortex which flows in the opposite direction to the primary vortex increases with an increase in Ha .
- By increasing the Lewis number, the heat transfer increases slightly for when $Ra = 10^3$ at $N = 2.0$. This condition is not observed for other Ra values. For all other situations, the heat transfer decreases with an increase in Lewis number.
- For $N = 2.0$ and $Ra = 10^4$, the heat transfer rate decrease of 26.34% is observed between $Le = 2.0$ and 10. For a similar condition for higher $Ra = 10^5$, the percentage decrease is 18.93%. But for the opposing buoyancy force ($N = -2.0$), for the same conditions, the percentage decrease obtained is 23.08% and 49.09% respectively.
- The mass transfer, however, increases with an increase in Lewis number for all the operating conditions. The fluid velocity also declines with increasing Lewis number.
- By decrement of Buoyancy, ratio causes a decline in heat and mass transfer rate. But after a critical value, the heat and mass transfer rate starts to increase again. The critical value changes concerning other operating conditions. It is observed that lower Ra the critical N value is 0.2 and -1.5 for heat and mass transfer respectively. For different Ra values, the heat and mass transfer rate decreases up to -1.5 and increases at -2. The nomenclature list should be in alphabetical order with Greek symbols, also in alphabetical order and with a separate heading, following the alphabetical listing. Subscripts and superscripts should follow Greek symbols and should be identified with separate headings.

Author Contributions

A. Sathiyamoorthi developed the LBM code using “C++” programming language and run the code for various operating conditions; S. Anbalagan also involved for developing the LBM code and compiled all the results for the present study; H.F. Oztop has discussed mathematical modeling section and examined the theoretical validations; N.H. Abu-Hamdeh contributed for preparing the manuscript and discussed the technical content of the paper. Finally, the manuscript was revised through the contribution of all authors and approved the final version of the manuscript in the present form.

Acknowledgments

Authors thank to the reviewers for giving excellent comments to improve the quality of the paper.

Conflict of Interest

The authors declared no potential conflicts of interest with respect to the research, authorship and publication of this article.

Funding

The authors received no financial support for the research, authorship and publication of this article.



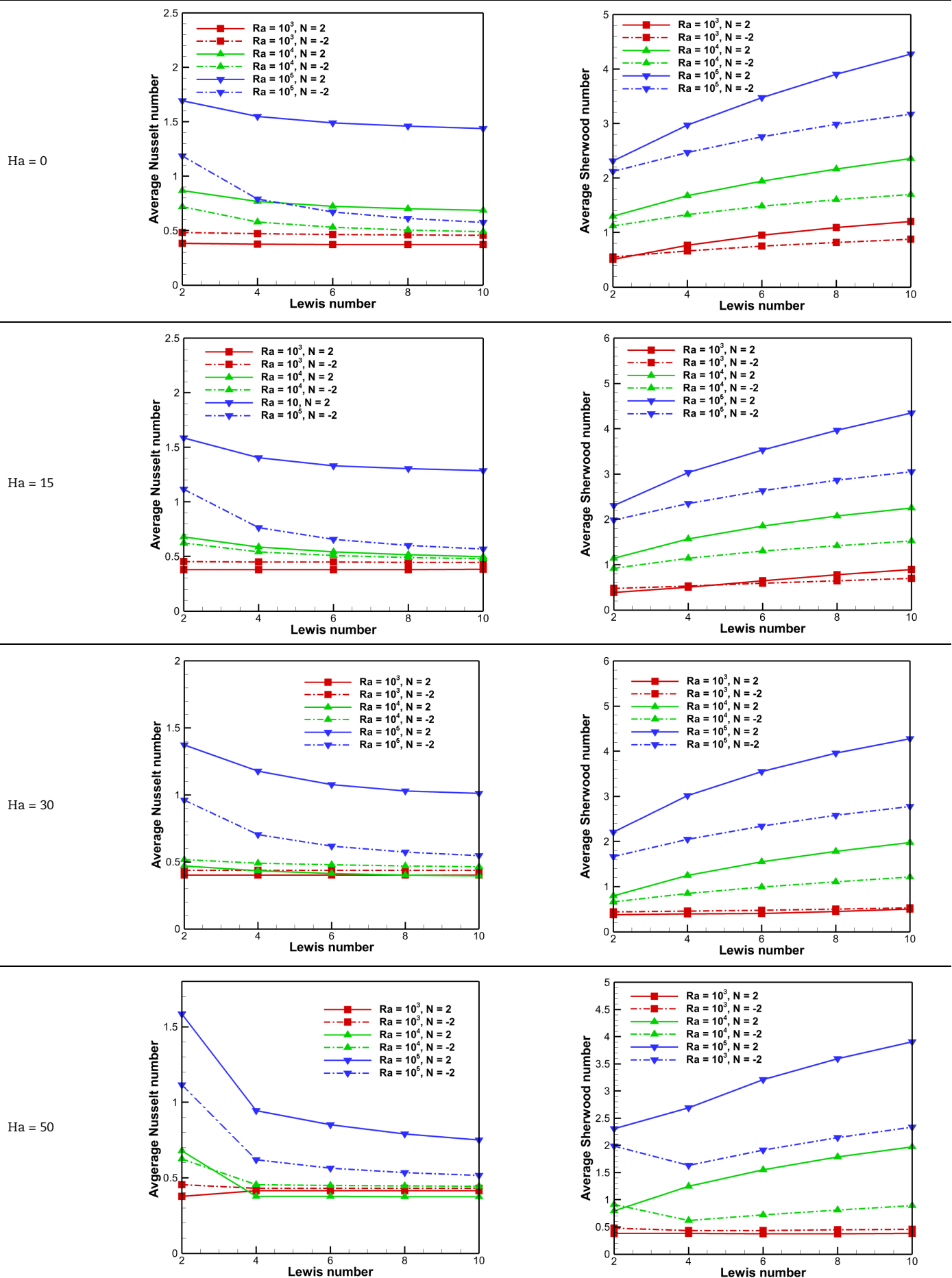



Fig. 13. Average Nusselt and Sherwood number for different Le, Ha, and Ra at $N = 2.0$ and -2.0





- [26] Mondal, S., Sibanda, P., Unsteady double diffusive convection in an inclined rectangular lid-driven enclosure with different magnetic field angles and non-uniform boundary conditions, *International Journal of Heat and Mass Transfer*, 90, 2015, 900-910.
- [27] Kumar, V., Murthy, S.V.S.S.N.V.G.K., Kumar, B.V.R., Influence of MHD forces on Bejan's heatlines and masslines in a doubly stratified fluid saturated Darcy porous enclosure in the presence of Soret and Dufour effects – A numerical study, *International Journal of Heat and Mass Transfer*, 117, 2018, 1041-1062.
- [28] Hussain, S., Oztog, H.F., Jamal, M., Hamdeh, N.A., Double diffusive nanofluid flow in a duct with cavity heated flow below, *International Journal of Mechanical Sciences*, 131-132, 2017, 535-545.
- [29] Sheikholeslami, M., Oztog, H.F., MHD free convection of nanofluid in a cavity with sinusoidal walls by using CVFEM, *Chinese Journal of Physics*, 55(6), 2017, 2291-2304.
- [30] Mehryan, S.A.M., Izadi, M., Chamkha, A.J., Sheremet, M.A., Natural convection and entropy generation of a ferrofluid in a square enclosure under the effect of a horizontal periodic magnetic field, *Journal of Molecular Liquids*, 263, 2018, 510525.
- [31] Purushothaman, P., Satheesh, A., Natural convection heat transfer and fluid flow analysis in a 2D square enclosure with sinusoidal wave and different convection mechanism, *International Journal of Numerical Methods for Heat and Fluid Flow*, 28(9), 2018, 2158-2188.
- [32] Teamah, M.A., Shehata, A.I., Magnetohydrodynamic double diffusive natural convection in trapezoidal cavities, *Alexandria Engineering Journal*, 55, 2016, 1037-1046.
- [33] Ghalambaz, M., Chamkha, A.J., Wen, D., Natural convective flow and heat transfer of Nano-Encapsulated Phase Change Materials (NEPCMs) in a cavity, *International Journal of Heat and Mass Transfer*, 138, 2019, 738-749.
- [34] Ghalambaz, M., Mehryan, S.A.M., Zahmatkesh, I., Chamkha, A., Free convection heat transfer analysis of a suspension of nano-encapsulated phase change materials (NEPCMs) in an inclined porous cavity, *International Journal of Thermal Sciences*, 157, 2020, 106503.
- [35] Hajjar, A., Mehryan, S.A.M., Ghalambaz, M., Time periodic natural convection heat transfer in a nano-encapsulated phase-change suspension, *International Journal of Mechanical Sciences*, 166, 2020, 105243.
- [36] Selimefendigil, F., Oztog, H.Z., Mixed convection and entropy generation of nanofluid flow in a vented cavity under the influence of inclined magnetic field, *Microsystem Technologies*, 25, 2019, 4427-4438.
- [37] Ratnadeep, N., Murugesan, K., Optimization of double diffusive mixed convection in a BFS channel filled with Alumina nanoparticle using Taguchi method and utility concept, *Scientific Reports*, 9, 2019, 19536, 1-19.
- [38] Yasmin, A., Ali, K., Ashraf, M., Study of Heat and Mass Transfer in MHD Flow of Micropolar Fluid over a Curved Stretching Sheet, *Scientific Reports*, 10, 2020, 4581, 1-11.
- [39] Bhatnagar, P.L., Gross, E.P., Krook, M., A model for collision processes in gases. I. Small amplitude processes in charged and neutral one-component systems, *Physical Review Journals Archive*, 94, 1954, 511-525.
- [40] Mohammed, A.A., *Lattice Boltzmann Method: Fundamentals and Engineering Applications with Computer Codes*, Springer, 2012.
- [41] Mohamad, A.A., Kuzmin, A., A critical evaluation of force term in lattice Boltzmann method, natural convection problem, *International Journal of Heat and Mass Transfer*, 53, 2010, 990-996.
- [42] Kefayati, G.R., Lattice Boltzmann simulation of MHD natural convection in a nanofluid-filled cavity with sinusoidal temperature distribution, *Powder Technology*, 243, 2013, 171-183.
- [43] Arun, S., Satheesh, A., Mesoscopic analysis of MHD double diffusive natural convection and entropy generation in an enclosure filled with liquid metals, *Journal of the Taiwan Institute of Chemical Engineers*, 95, 2019, 155-173.

ORCID iD

Arun Sathiyamoorthi  <https://orcid.org/0000-0001-5690-6299>

Satheesh Anbalagan  <https://orcid.org/0000-0001-5045-5263>

Hakan F. Oztog  <https://orcid.org/0000-0002-2161-0639>

Nidal H Abu-Hamdeh  <https://orcid.org/0000-0002-4852-2217>



© 2021 Shahid Chamran University of Ahvaz, Ahvaz, Iran. This article is an open access article distributed under the terms and conditions of the Creative Commons Attribution-NonCommercial 4.0 International (CC BY-NC 4.0 license) (<http://creativecommons.org/licenses/by-nc/4.0/>).

How to cite this article: Sathiyamoorthi A., Anbalagan S., Oztog H.F., Abu-Hamdeh N.H. MHD Double-Diffusive Natural Convection in a Closed Space Filled with Liquid Metal: Mesoscopic Analysis, *J. Appl. Comput. Mech.*, 7(3), 2021, 1448-1465. <https://doi.org/10.22055/JACM.2020.33719.2273>

Publisher's Note Shahid Chamran University of Ahvaz remains neutral with regard to jurisdictional claims in published maps and institutional affiliations.

